2D hyperbolic groups induce three-periodic euclidean reticulations

Vanessa Robins, Stuart Ramsden, Stephen Hyde

Department of Applied Mathematics, Research School of Physical Sciences,

The Australian National University, Canberra ACT 0200, Australia.

April 2, 2004

Abstract

Many crystalline networks can be viewed as decorations of triply periodic minimal surfaces. Such surfaces are covered by the hyperbolic plane in the same way that the euclidean plane covers a cylinder. Thus, a symmetric hyperbolic network can be wrapped onto an appropriate minimal surface to obtain a 3d periodic net. This requires symmetries of the hyperbolic net to match the symmetries of the minimal surface. We describe a systematic algorithm to find all the hyperbolic symmetries that are commensurate with a given minimal surface, and the generation of simple 3d nets from these symmetry groups.

Keywords: Hyperbolic tilings, minimal surfaces, networks, frameworks, reticular chemistry, symmetry groups

PACS: 61.50.Ah, 89.75.Hc, 02.20.-a, 02.40.-k

1 Introduction

Network, or *reticular*, models are widely used descriptions of three-dimensional structure in chemistry. Nature provides a rich set of examples for us to study, e.g. the covalent bonding structure of crystalline minerals, the alumino-silicate backbone of zeolites, and metal-organic frameworks. Chemists interested in synthesizing materials with particular properties need to know what structures are possible, and which are the most likely to form. Systematic techniques for generating 3D periodic networks are still being developed and are yet to provide a complete enumeration of possible network structures[1, 2, 3, 4, 5]. Our approach generates 3D euclidean networks by wrapping 2D hyperbolic nets onto triply periodic minimal surfaces (TPMS). Formally this is done by constructing a covering map from the hyperbolic plane onto the minimal surface. Periodic 3D nets are obtained only when the symmetries of the hyperbolic net and the covering map are commensurate with the symmetries of the surface. This paper focusses on group theoretic aspects of the projection from 2D hyperbolic space into 3D euclidean space. The work follows a number of earlier explorations of the route to 3D structure from 2D curved space; a brief overview follows.

We view 3D crystalline reticulations as *decorations* of TPMS — a concept that was recognised first by solid state chemists 20 years ago as a clue to understanding complex covalent frameworks, particularly alumino-silicate zeolites and related materials [6, 7]. More recent advances in the differential geometry of TPMS [8] and in tiling theory [9, 10, 11, 12] are proving indispensable to progress. The euclidean geometry of a TPMS is governed by the property that its Gauss map (the map of surface normal vectors) is a tiling of the 2-sphere. Indeed, an enumeration of simple "regular" TPMS arises by deriving all discrete tilings of the 2-sphere [13]. The symmetries of the Gauss map are readily "mutated" to deduce the in-surface 2D hyperbolic group of the resulting TPMS. The advent of *orbifold* theory by Macbeath and Thurston[14], and its later simple description using the notation invented by Conway[15, 16] allows for efficient numerical coding of 2D hyperbolic groups as well as exhaustive enumeration of allowed hyperbolic tilings with specified orbifold symmetry[11]. We combine tiling theory with the intrinsic geometry of TPMS to build tilings of TPMS and use the tiling topology to define embedded crystalline reticulations of 3D space. Some results have been described earlier [17, 18, 19].

The work described here continues the above investigations, with an emphasis on the group theoretic aspects of the problem. The prime motivation is to enumerate all allowed symmetries of tilings or reticulations on a particular TPMS that retain the translational symmetries of the oriented surface. This relies on identifying the full group structure of the TPMS (its "hyperbolic crystallography"), derived previously for the primitive (P), diamond (D), and gyroid (G) surfaces by Sadoc and Charvolin[20]. The examples below are limited to these simplest cubic genus-three TPMS [8]. The approach

is generic, however, and can be extended to arbitrarily complex TPMS, once their hyperbolic crystallography is known.

2 Covering maps for TPMS

The fundamental tool in our generation of 3D nets is a map that wraps up the hyperbolic plane onto the periodic minimal surface, $f : \mathbb{H}^2 \to M$. The pairing of the hyperbolic plane with this map is called a *cover*. (The existence of this map is guaranteed by fundamental results from topology[21].) A cover is a useful tool for many reasons — the covering space, $\mathbb{H}^2$, has simpler topology than the original surface, M, and properties of M can be determined from the action of the covering map, f. Specifically, it is much simpler to study symmetry groups and generate nets in the hyperbolic plane than in 3D euclidean space. The complexity is shifted to finding an appropriate covering map. The next few paragraphs describe this process.

There are many possible ways to define the covering map $f : \mathbb{H}^2 \to M$. We require that the cover respect the symmetries of the given minimal surface, i.e., the intrinsic local surface symmetry and the euclidean three-dimensional translational symmetry. In essence, we define f using an "orbifold chart" that maps a patch of the hyperbolic plane onto the related surface asymmetric unit patch. This map of a single orbifold patch extends to a map of the whole hyperbolic plane onto the whole TPMS via a correspondence of the symmetry operations, i.e. via a group homomorphism. Importantly, the euclidean translational symmetries of the TPMS pull back to hyperbolic translations. Thus, the definition of f is made almost entirely by reference to the symmetry group action. This process is best elaborated using an example.

The P, D, and G surfaces (illustrated in Figure 1) each have intrinsic surface symmetry related to the *246 hyperbolic reflection group. This relationship has a mathematical basis in the complex analytic Weierstrass-Enneper formula used to define these minimal surfaces — they are related via a Bonnet transformation. The implications of this for the crystallography of the P, D, G surfaces is explored in [22]. The *246 hyperbolic group is generated by three reflections, R_1, R_2, and R_3 whose mirror lines bound a triangle in $\mathbb{H}^2$ with corner angles of $\pi/2, \pi/4$, and $\pi/6$. By applying these operations in all possible combinations, images of the initial triangle cover the entire hyperbolic plane. Of course, not every word over $\{R_1, R_2, R_3\}$ gives a unique image, there is a set of relations for the group generated by the following: $R_1^2 = R_2^2 = R_3^2 = I$ (the identity) and $(R_1 R_2)^2 = (R_2 R_3)^4 = (R_1 R_3)^6 = I$.

Sadoc and Charvolin[20] found that these three closely-related surfaces each have a disk-like translational patch in $\mathbb{E}^3$, and that these pull back to the same dodecagon in the hyperbolic plane, as illustrated in Figure 2. There are six hyperbolic translations that pair opposite edges of the dodecagon, and generate a normal subgroup of *246 with orbifold symbol ooo. The translations were defined in [20] and are rewritten here in terms of the *246 reflections:

$$t_1 = (R_3 R_1 R_3 R_1 R_3 R_2)^2 \tag{1}$$
$$t_2 = R_3 R_1 R_3 t_1 R_3 R_1 R_3$$
$$t_3 = (R_1 R_3)^2 t_1 (R_3 R_1)^2$$
$$\tau_1 = (R_3 R_1 R_2)^2 (R_3 R_1)^2 R_2 R_3 R_2 R_1 R_3 R_1$$
$$\tau_2 = R_1 R_3 R_1 \tau_1 R_1 R_3 R_1$$
$$\tau_3 = R_3 \tau_1 R_3.$$

These translations satisfy the following identity in $\mathbb{H}^2$:

$$\tau_1 t_2 \tau_3^{-1} t_1^{-1} \tau_2 t_3 \tau_1^{-1} t_2^{-1} \tau_3 t_1 \tau_2^{-1} t_3^{-1} = I. \tag{2}$$

Each surface has a different covering map that can be compactly described by defining how the hyperbolic translations above map to euclidean translations. For the P-surface, $f_P(t_1), f_P(t_2)$, and $f_P(t_3)$ are linearly independent in $\mathbb{E}^3$ and commute, with

$$f_P(\tau_1) = f_P(t_2^{-1} t_3), \tag{3}$$
$$f_P(\tau_2) = f_P(t_3^{-1} t_1), \text{and}$$
$$f_P(\tau_3) = f_P(t_1^{-1} t_2).$$

For the D-surface $f_D(t_1), f_D(t_2)$, and $f_D(\tau_3)$ are a commuting linearly independent set, with

$$f_D(t_3) = f_D(t_3^{-1} t_2^{-1}), \tag{4}$$
$$f_D(\tau_2) = f_D(t_1 \tau_3), \text{and}$$
$$f_D(\tau_1) = f_D(t_2^{-1} \tau_3).$$

Lastly, for the Gyroid, $f_G(t_1), f_G(t_2)$, and $f_G(t_3)$ are again independent with

$$f_G(\tau_1) = f_G(t_1^{-1} t_2^{-1}), \tag{5}$$
$$f_G(\tau_2) = f_G(t_2^{-1} t_3^{-1}), \text{and}$$
$$f_G(\tau_3) = f_G(t_3^{-1} t_1^{-1}).$$

In the following section we explain how these hyperbolic groups and covering maps are used to find all symmetry groups commensurate with a given surface.

3 Enumeration of commensurate symmetries

Our goal is to find all sub-symmetries, G, that are commensurate with the intrinsic symmetry, S, of a given
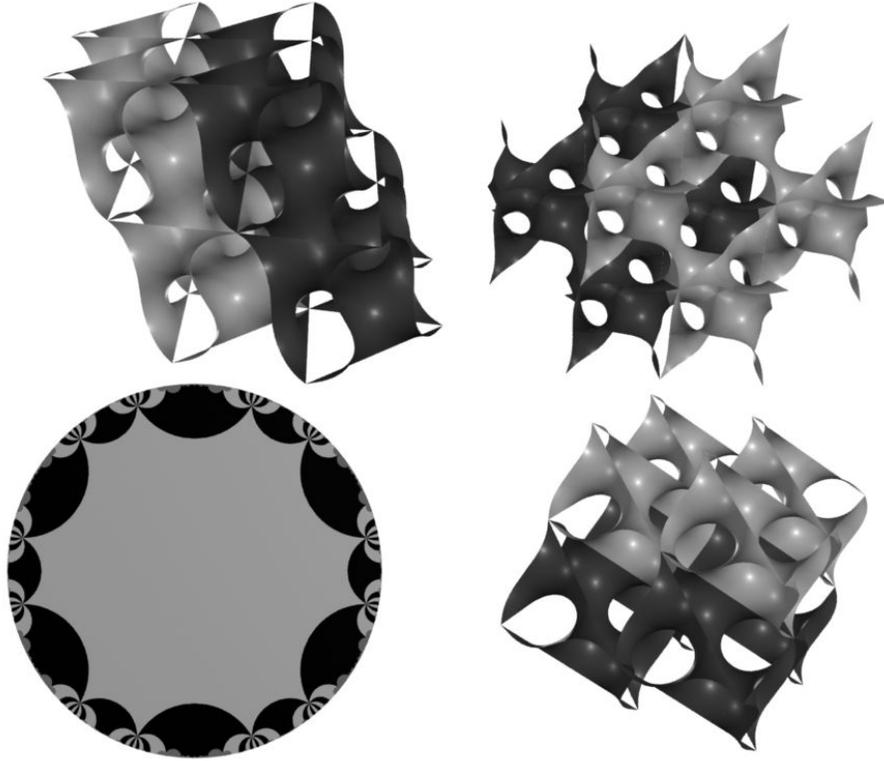
Figure 1: *Anticlockwise from bottom left:* A tiling of the hyperbolic plane by dodecagons, twelve around each vertex; the P, G, and D minimal surfaces built from the translational units in Figure 2.

minimal surface. Algebraically, G must be a subgroup of S and a supergroup of the euclidean translation group, T. An elementary result from group theory[23] tells us that such groups G satisfying $T \subset G \subset S$ are in one-to-one correspondence with subgroups of the quotient group: $\tilde{G} \subset S/T$.

The covering maps defined in the previous section allow us to work with hyperbolic groups rather than the more complex surface groups. For the P, D and G surfaces, we must enumerate all subgroups of

$$*246/[t_1 = t_2 = \cdots = \tau_3 = I].$$

Although the hyperbolic group *246 is infinite, the quotient group is finite, so enumerating these subgroups is a simple matter for the computational discrete algebra package, GAP (Groups, Algorithms and Programming)[24]. The result from GAP is a list of finitely presented groups, with generators in the quotient group. Adding back in the hyperbolic translation subgroup generators, $\{t_1, \ldots, \tau_3\}$ and using GAPs group isomorphism tools, gives us a list of finitely presented subgroups of *246.

There is no unique way to represent such groups, and we encounter the perpetual problem of group theory: finding an isomorphism from a given group to a canonical form. In this context, however, there is a solution — discrete groups of isometries of the sphere, euclidean, and hyperbolic plane are characterised by their orbifold (the "orbit manifold" defined by Thurston[14]). Conway devised an elegant symbolic notation that encodes the orbifold structure[15, 16]. We give a brief synopsis of this notation in appendix A. The orbifold symbol is easily computed from any tiling with the given group symmetry[12]. Therefore, we construct a tiling for each subgroup and then compute the orbifold symbol from this tiling.

We start by building the fundamental tiling for the hyperbolic surface group *246. This tiling consists of the black and white triangles illustrated in Figure 2. Each triangle is labelled by the element of *246 that maps a fixed initial triangle onto this new triangle. We obtain a unique minimal word for each group element using word enumeration and reduction algorithms (for example via the KBMAG package [25] which is an extension to GAP). The adjacency information for the triangles is induced from the initial triangle neighbours as follows. Recall that the initial triangle is bounded by the mirror lines for the three reflections R_1, R_2, and R_3 so the three
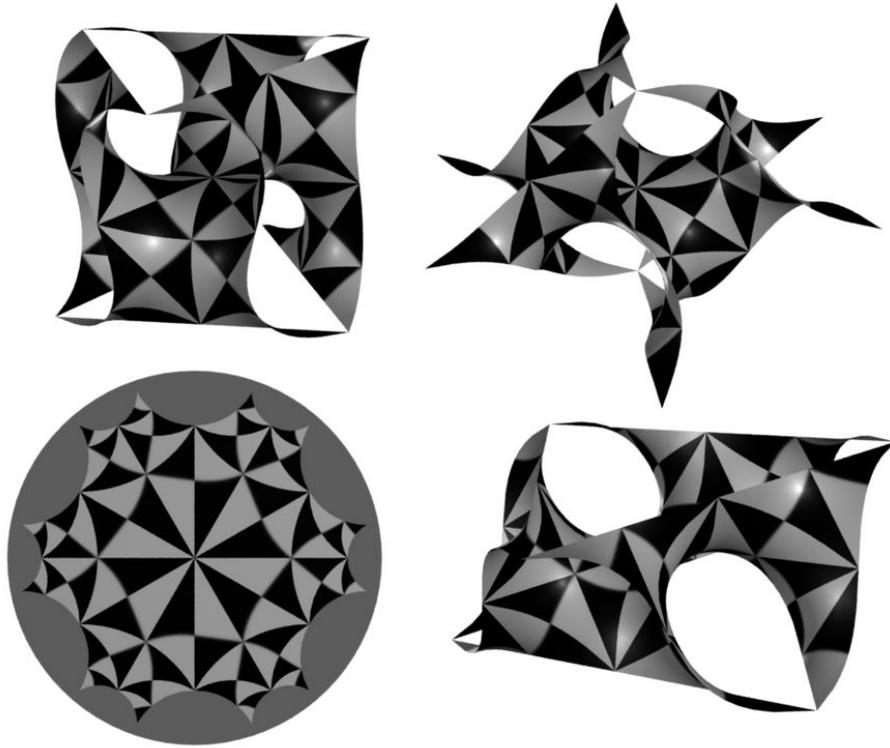
Figure 2: *Anticlockwise from bottom left:* The dodecagonal translational patch in the hyperbolic plane; corresponding surface patches for the P, G, and D minimal surfaces. The black and grey triangles are *246 fundamental domains — there are 96 such triangles in the dodecagonal translation unit, corresponding to the 96 elements of *246/ooo.

neighbouring triangles will have the labels R_1, R_2, and R_3. We then map this adjacency pattern to each image of the initial triangle: the triangle R_1 will therefore have the neighbours $R_1^2 = I, R_2 R_1, R_3 R_1$, and so on.

For a given subgroup, we use coset word enumeration algorithms from KBMAG to determine which elements of *246 are equivalent under the subgroup action. (The triangles in the original fundamental tiling are all equivalent under *246, so the subgroup action breaks this symmetry.) The subgroup fundamental domain is a grouping of non-equivalent *246 triangles. The grouping is not unique (except for kaleidoscopic groups where the orbifold symbol has the form *abc...) but KBMAG always gives an initial subgroup domain corresponding to the non-equivalent words of minimal length. Any particular choice of subgroup domain generates a new tiling of $\mathbb{H}^2$, with tile adjacency induced by the original *246 triangle adjacencies. Finally we use combinatorial tiling algorithms[12] to compute the orbifold symbol. The results of this process are presented in Table 1 of Appendix B. Further information is available online [26] where we present a graph of the relationships between

subgroups and illustrations of each subgroup symmetry in the hyperbolic plane.

4 From subgroup domains to periodic nets

Once we know the subgroup domains and their adjacency pattern it is straightforward to generate a vertex-transitive net with the symmetry of the subgroup. This is achieved by putting a single vertex in each subgroup domain, then joining vertices by an edge if the two domains are adjacent. The result is a periodic net in the hyperbolic plane. Note that this net is not unique for a given subgroup because the choice of subgroup domain is non-unique.

Careful use of word reduction with respect to the translation subgroup T gives us explicit knowledge of the translational unit for the hyperbolic net and the connections between nodes in successive translational cells. For example, the following hyperbolic net comes from the 22222222 (2^8) orbifold, with vertex 1 being in the iden-

tity domain, I, and vertex 2 in $(R_1 R_3)^3$:

$$
\begin{array}{cccccc}
1 & 1 & \tau_1, & 1 & 2 & I, \\
1 & 2 & t_1^{-1}, & 1 & 2 & t_2, \\
1 & 2 & t_3, & 1 & 2 & \tau_2^{-1}, \\
1 & 2 & \tau_3, & 2 & 2 & \tau_1.
\end{array}
$$

Each triple above represents an edge: the first entry denotes one vertex in the initial translational cell and the other two entries denote the second vertex type and its cell location.

The hyperbolic net topology is easily translated into a three-dimensional euclidean net topology via the covering map. To map the above net onto the P surface we can set $f_P(t_1), f_P(t_2), f_P(t_3)$ to the unit x, y, z-translations respectively, with the τ_i defined as in (3). The euclidean net topology is then

$$
\begin{array}{cccccc}
1 & 1 & (0,-1,1) & 1 & 2 & (0,0,0) \\
1 & 2 & (-1,0,0) & 1 & 2 & (0,1,0) \\
1 & 2 & (0,0,1) & 1 & 2 & (-1,0,1) \\
1 & 2 & (-1,1,0) & 2 & 2 & (0,-1,1)
\end{array}
$$

Now that we have the net topology, we need to assign coordinates to the vertices. This can be done in a number of ways including (i) a direct map from the hyperbolic plane onto the periodic minimal surface[17, 27], (ii) equilibrium (or barycentric) placements[28], or (iii) relaxation according to an energy potential that is minimized by equal edge-lengths and angles[13].

5 Isomorphic subgroups

A close examination of Table 1 shows that many subgroups occur as conjugate families, and that the same orbifold symbol can appear more than once. Two subgroups with the same orbifold symbol are isomorphic so are different representations of the same abstract symmetry. A net with a given symmetry which is mapped into two isomorphic subgroups gives two hyperbolic nets that are necessarily isomorphic in $\mathbb{H}^2$, but this isomorphism may be broken once they are projected into $\mathbb{E}^3$. Whether or not the subgroup isomorphism is preserved can be determined by studying the action of the isomorphism on the surface relations induced by the covering map.

First consider the case of conjugate subgroups, $A, B \subset S$, the surface-intrinsic symmetry group. Geometrically, conjugate subgroups appear as exactly the same pattern in $\mathbb{H}^2$ only shifted with respect to the original identity element of S. Algebraically it means that there is a fixed group element, $r \in S$ such that for every $a \in A$, there is a $b \in B$ with $a = rbr^{-1}$. Now consider the subgroup of A generated by the surface relations $R_A = \{r_{A1}, r_{A2}, \ldots r_{An}\}$, these elements of A map to the identity in $\mathbb{E}^3$ under the covering map: $f(r_{Ai}) = I$. Under the conjugacy operation this subgroup of A maps to a subgroup of B, with generating elements $R_B = \{rr_{A1}r^{-1}, \ldots, rr_{An}r^{-1}\}$. Then the covering map acts as follows: $f(rr_{Ai}r^{-1}) = f(r)f(r_{Ai})f(r^{-1}) = f(r)If(r)^{-1} = I$. It follows that R_B defines the same surface relations as R_A, and therefore conjugate subgroups give rise to isomorphic patterns in $\mathbb{E}^3$.

Next we examine the case of isomorphic, non-conjugate subgroups, G and $H \subset S$. Although G and H have the same orbifold symbol, they sit inside the parent group S differently and the patterns of their subgroup domains in $\mathbb{H}^2$ are not isometric. Let the isomorphism between the groups be $\phi : G \to H$, and let R_G, R_H denote the surface-relation subgroups expressed in G- and H-elements respectively. Then the covering map preserves the isomorphism of G and H only in the case that $\phi(R_G) = R_H$.

As an example, we present vertex-transitive nets derived from two subgroups with orbifold *2244 (numbers 103 and 107 in Table 1). The pattern of the subgroup domains and corresponding 3D nets are illustrated in Figure 3. We can see directly from the pattern of subgroup domains that there is no isomorphism from one group to the other that preserves the translational unit. In subgroup 107, a long edge of the dodecagon passes along the $\pi/4 - \pi/4$ edge of a subgroup domain, but this is not the case in the other subgroup, 103. The four-coordinated vertex-transitive nets that arise from these subgroups have 4-rings and 8-rings in the hyperbolic plane, and the projection into $\mathbb{E}^3$ produces 4-rings in one case, and 6-rings in the other. We recognize the net from subgroup 107 as being the alumino-silicate backbone of the zeolite ACO [29] and the net derived from subgroup 103 as ATN [30].

Finally, we study what happens when a given subgroup is mapped onto two different surfaces. This situation is analogous to the previous one, except that we must study an automorphism of the subgroup onto itself, rather than an isomorphism between two different versions of the same symmetry. If there is an automorphism of the subgroup that maps one set of surface relations onto the other surface relations (e.g. the P onto the D) then we will get isomorphic patterns in $\mathbb{E}^3$, otherwise not.

We finish with a simple example of three different nets obtained from the same hyperbolic pattern of four regular hexagonal tiles meeting at each vertex (illustrated in Figure 4). The hyperbolic net can arise as the vertex-transitive fundamental net for the 6222 group (number 93 in Table 1), and also from non-fundamental tilings
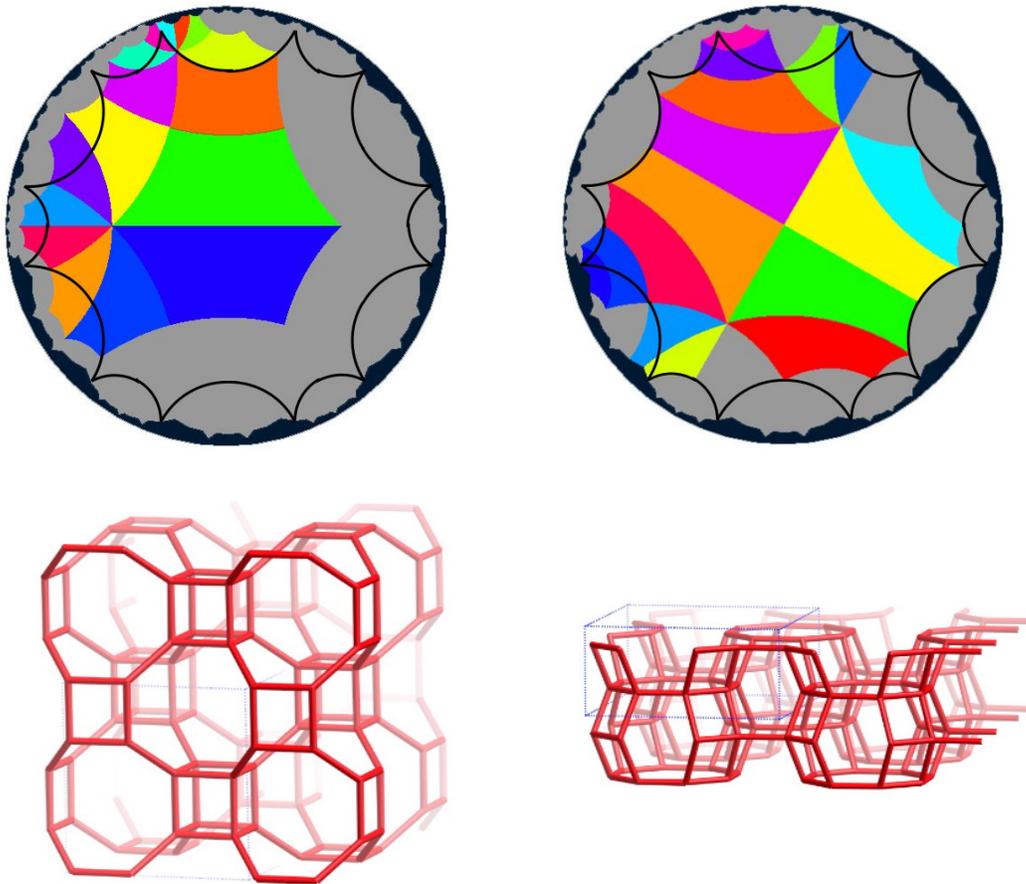
Figure 3: *Top:* Two subgroup domain patterns with orbifold symbol *2244 (left image is from subgroup 107, right from 103 in Table 1). These kaleidoscopic subgroup domains are fixed by mirror lines that bound a quadrilateral with corner angles $\pi/2, \pi/2, \pi/4, \pi/4$. Each subgroup domain is assigned a different colour (seen in the electronic version). In each case the coloured region is a single translation domain of the subgroup T, and has the same area as the original dodecagon (shown as the black outline). *Bottom:* The corresponding vertex-transitive nets projected onto the P surface and then relaxed to equalize edge lengths and angles.

of higher symmetry. When mapped onto the P,D, and G surfaces respectively, we obtain frameworks familiar to solid state chemists as the aluminosilicate backbone of sodalite (the zeolite SOD)[31, p.315], niobium oxide, NbO[31, p.316], and S* (a lattice complex derived from an 8-coordinated sphere packing)[31, p.320] and [32, Table 14.3].

6   Conclusions

The output of this approach — 3D crystalline reticulations — is similar to that of the program of O'Keeffe, Friedrichs *et al.*[3, 4, 5]. The latter use tiling theory in 3D euclidean space, we confine tiling aspects to 2D hyperbolic space. Both approaches have relative advantages and disadvantages. The 3D euclidean approach is intuitively more clear, at the (considerable!) expense of having to work in three flat instead of two curved dimensions. Our technique is limited by the choice of TPMS, but extends to include multiple interwoven networks as well as rod and helical packings[33]. Most importantly, both techniques produce very large lists of examples once the allowed symmetries of reticulations in 3D are decreased (Friedrichs' approach) or TPMS genus increases (our approach). Sensible filters must be applied for practical purposes. Those filters result in complementary results for both approaches, with significant overlap for the simplest examples. These reasons encourage us to continue on our path.
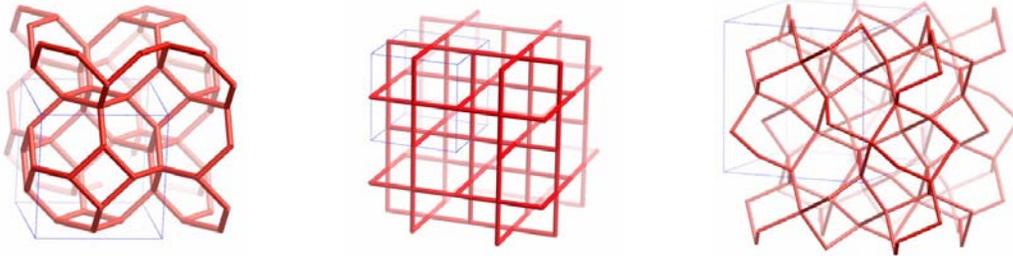
Figure 4: The hyperbolic net with Schläfli symbol 6.6.6.6 is projected onto the P, D, and G surfaces to give 3D euclidean nets *sodalite, NbO,* and *S**.

Acknowledgments

A Conway's orbifold notation for 2D discrete groups

Every discrete group of symmetries, S, acting on a 2D space of constant curvature K (i.e. $\mathbb{H}^2, E^2, S^2$) is uniquely characterised by its "orbit manifold" or *orbifold* — a quotient of K by the action of S. Two-dimensional symmetries are rotations about a point, reflections in (possibly intersecting) mirror lines, translations, and glide reflections. These induce cone points, boundaries, handles and cross-caps in the orbifold. An orbifold is therefore a compact connected 2d manifold with boundary. Any such manifold is described by starting with a sphere, removing discs to generate boundary components, then adjoining handles or cross-caps. The orbifold symbol is a compact encoding of this topology and has the general form: o...oABC...*ab...*st...x...x. The special symbols o,*, and x represent the topological features of a handle, boundary component, and cross-cap respectively. An orbifold has a metric induced from its parent space, K, so it can also have distinguished points. In particular, the upper-case letters represent cone points where the total surface angle is $2\pi/A$, rather than 2π. The lower-case letters following each star, *ab..., list corner angles $\pi/a, \pi/b$, as they occur in cyclic order around a boundary component. For example, o** is a torus with two smooth boundary components; *22*22 is a cylinder for which both boundary components have two corners of $\pi/2$; 22xx has two cone points of order 2 (angle π) and two cross-caps.

B The commensurate subgroups

In this appendix we present the subgroups commensurate with the P, D, and G surfaces. In Table 1 we list each subgroup orbifold, its index in *246, the number of conjugate subgroups of this symmetry, and generators for the subgroup in the quotient group *246/T (the translations in (1) must be added to obtain generators for the full group). There is a complex set of relations between these subgroups which is illustrated by a graph of the maximal subgroup lattice shown in Figure 5. This lattice is also available in a large high-resolution format via the online supplementary material [26]. In the online material each node of the lattice links to a subgroup record. We include four sets of example images from these subgroup records in Figure 6. These examples illustrate the variety of symmetry operations that occur in the subgroups from translations to glide reflections, rotations and reflections of orders 2,3,4,and 6.

References

[1] S.J. Chung, Th. Hahn, and W.E. Klee. *Acta Cryst. A*, 40:42–50, 1984.

[2] M. Bader, W.E. Klee, and G. Thimm. *Z. Kristallog.*, 214:553–558, 1997.

[3] O. Delgado-Friedrichs, A.W.M. Dress, D.H. Huson, J. Klinowski, and A.L. Mackay. *Nature*, 400:644–647, 1999.

[4] O. Delgado-Friedrichs, M. O'Keeffe, and O.M. Yaghi. *Acta Cryst. A*, 59:22–27, 2003.

[5] O. Delgado-Friedrichs, M. O'Keeffe, and O.M. Yaghi. *Acta Cryst. A*, 59:515–525, 2003.

[6] S. Andersson. *Angewandte Chemie. Int. Ed. Engl.*, 22:69–81, 1983.

[7] A. Mackay. In *International Union of Crystallography Copenhagen meeting*, 1979.

[8] A. Fogden and S.T. Hyde. *Acta Cryst. A*, 48:442–451, 1992.

[9] A.W.M. Dress. *Advances in Mathematics*, 63:196–212, 1987.

[10] A.W.M. Dress and D.H. Huson. *Geometriae Dedicata*, 24:295–310, 1987.

[11] L. Balke and D.H. Huson. *Geometriae Dedicata*, 60:89–106, 1996.

[12] O. Delgado-Friedrichs. *Theoretical Computer Science*, 303:431–445, 2003.

[13] S.T. Hyde, S. Ramsden, T. DiMatteo, and J. Longdell. *Solid State Sciences*, 5:35–45, 2003.

[14] W.P. Thurston. Princeton University Press, 1980.

[15] J.H. Conway. In *Groups, combinatorics, and geometry*, volume 165 of *LMS Lecture Notes*, pages 438–447. Cambridge University Press, 1992.

[16] J.H. Conway and D.H. Huson. *Structural Chemistry*, 13:247–256, 2002.

[17] S.T. Hyde and S. Ramsden. In D. Bonchev and D.H. Rouvray, editors, *Chemical Topology: Applications and Techniques*, chapter 2, pages 35–173. Gordon and Breach Science, Amsterdam, 2000.

[18] S.T. Hyde and C. Oguey. *European Physical Journal B*, 16:613–630, 2000.

[19] S.T. Hyde and S. Ramsden. *European Physical Journal B*, 31:273–284, 2003.

[20] J.-F. Sadoc and J. Charvolin. *Acta Cryst. A*, 45:10–20, 1989.

[21] W.S. Massey. *A basic course in algebraic topology*. Springer, New York, 1991.

[22] C. Oguey and J.-F. Sadoc. *Journal de Physique I*, 3:839–854, 1993.

[23] I.N. Herstein. *Topics in Algebra*. Blaisdell, Waltham, MA, 1964.

[24] The GAP Group. *GAP – Groups, Algorithms, and Programming, Version 4.3*, 2002. `www.gap-system.org`.

[25] D.F. Holt. *KBMAG — Knuth-Bendix for Monoids and Automatic Groups Version 2.4*. University of Warwick, 1998. `ftp.maths.warwick.ac.uk/people/dfh/kbmag2/`.

[26] V. Robins, S. Ramsden, and S.T. Hyde. Symmetries of the P,D, and G minimal surfaces, 2004. `wwwrsphysse.anu.edu.au/~vbr110/PDGdata/`.

[27] S.T. Hyde and S. Ramsden. *DIMACS Series in Discrete Mathematics and Theoretical Computer Science*, 51:203–224, 2000.

[28] O. Delgado-Friedrichs and M. O'Keeffe. *Acta Cryst. A*, 59:351–360, 2003.

[29] P.Y. Feng, X.H. Bu, and G.D. Stucky. *Nature*, 388:735–741, 1997.

[30] L.B. McCusker, G.O. Brunner, and A.F. Ojo. *Acta Cryst. A*, 46:C59, 1990.

[31] M. O'Keeffe and B.G. Hyde. *Crystal Structures I. Patterns and Symmetry*. Mineralogical Society of America, Washington, DC, 1996.

[32] T. Hahn, editor. *International Tables of Crystallography*, volume A. Kluwer, Dordrecht, third edition, 1992.

[33] S.T. Hyde, A.-K. Larsson, T. DiMatteo, S. Ramsden, and V. Robins. *Australian Journal of Chemistry*, 56:981–1000, 2003.
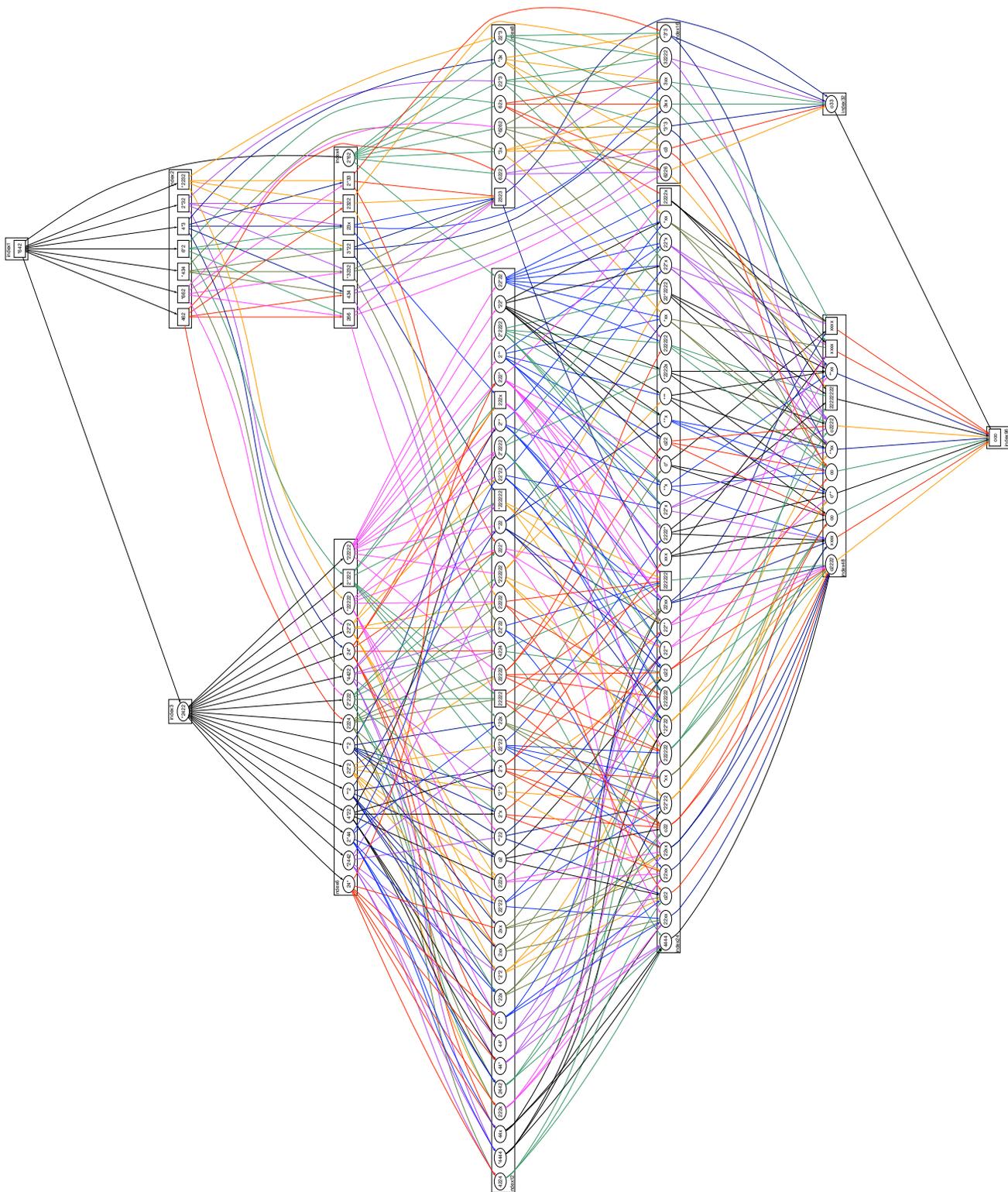
Figure 5: The lattice of maximal subgroup relations for the 131 conjugacy classes of Table 1.
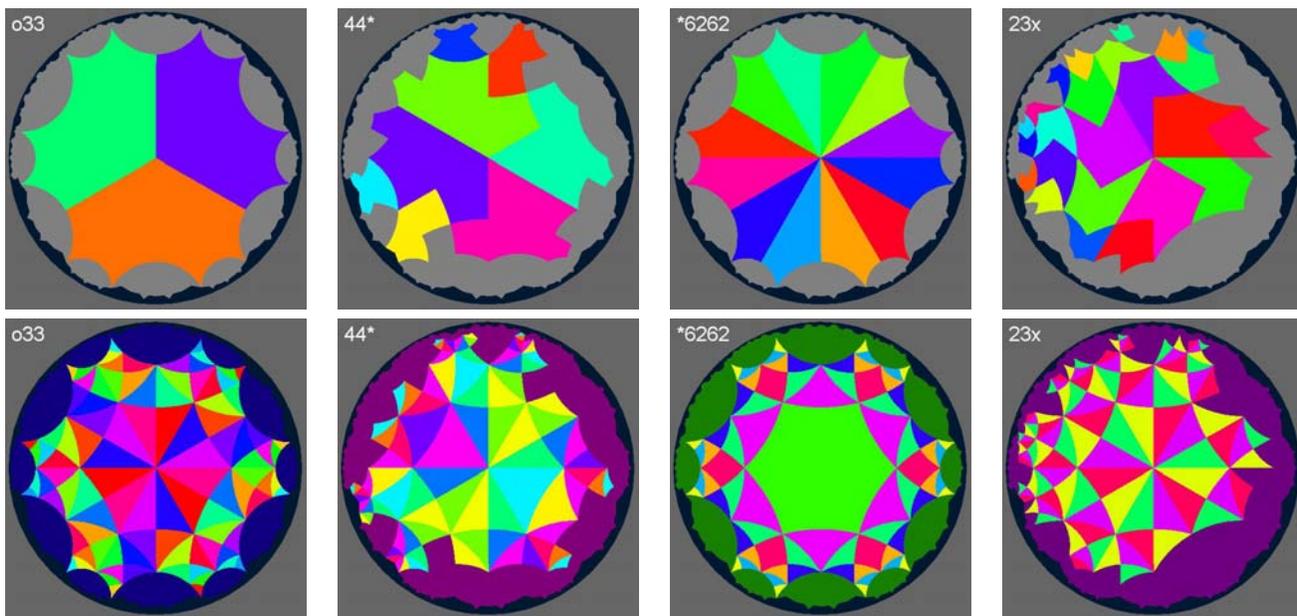
Figure 6: Each frame above shows a Poincaré disc with a coloured region of 96 *246 triangles — an area equal to that of the translation unit dodecagon. In the *top row* the colours are assigned so that each subgroup domain has a different colour. In the *bottom row* the colours are assigned so that *246 triangles have the same colour when they are equivalent under the subgroup symmetry action.

Table 1: Subgroups of *246 commensurate with the P,D,G surfaces.

|	orbifold symbol	index	conjugacy class size	subgroup generators in *246/T
1	ooo	96	1	identity
2	22222222	48	1	$R_3R_1R_3R_1R_3R_1$
3	xxxx	.	.	$R_1R_2R_3R_2R_3R_1R_3R_2R_3$
4	xxxx	.	.	$R_1R_2R_3R_1R_2R_3R_2R_1R_3$
5	xxxx	48	3	$R_1R_2R_3R_1R_3R_1R_3$
6	o**	.	.	R_2
7	o2222	.	.	$R_3R_2R_3R_2$
8	oo	.	.	$R_2R_3R_1R_3R_2R_1R_3R_1$
9	**xx	48	6	R_1
10	**xx	.	.	R_3
11	o2222	.	.	R_2R_1
12	oo	.	.	$R_3R_1R_3R_1R_3R_2$
13	o33	32	4	$R_3R_1R_3R_1$
14	222222	24	1	$R_3R_2R_3R_2, R_1R_3R_2R_3R_2R_1$
15	2222x	.	.	$R_3R_1R_3R_1R_3R_1, R_1R_2R_3R_1R_2R_3R_2R_1R_3$
16	222222	24	3	$R_2R_1, R_3R_1R_3R_2R_3R_2R_1R_3$
17	4444	.	.	R_3R_2
18	o22	.	.	$R_3R_2R_3R_2, R_1R_3R_1R_3R_2R_1$
19	22xx	.	.	$R_3R_2R_3R_2, R_1R_2R_3R_1R_2R_3R_1$
20	22**	.	.	$R_1, R_3R_1R_3R_2R_3R_2R_1R_3$
21	o22	.	.	$R_3R_2R_3R_2, R_3R_1R_3R_2R_3R_1$
22	22**	.	.	$R_2, R_3R_1R_3R_2R_3R_2R_1R_3$
23	2222*	.	.	$R_2, R_3R_1R_3R_1R_3R_1$
24	o22	.	.	$R_3R_2R_3R_2, R_2R_3R_1R_3R_2R_1R_3R_1$
25	*22*22	.	.	$R_2, R_3R_2R_3$
26	22xx	.	.	$R_3R_2R_3R_2, R_1R_2R_3R_2R_3R_1R_3$
27	222222	.	.	$R_3R_2R_3R_2, R_3R_1R_3R_1R_3R_1$
28	*22*22	.	.	$R_3, R_2R_3R_2$
29	22xx	.	.	$R_3R_2R_3R_2, R_1R_2R_3R_1R_3R_1R_3$
30	o*	.	.	$R_2, R_3R_1R_2R_3R_2R_1R_3R_1$
31	xxx	.	.	$R_1R_2R_3R_1R_3R_1R_3, R_3R_1R_2R_3R_2R_1R_3R_1$
32	22xx	.	.	$R_3R_2R_3R_2, R_1R_3R_1R_2R_3R_1R_3$
33	**x	24	6	$R_1, R_3R_1R_3R_1R_3R_2$
34	*2222x	.	.	R_1, R_2
35	22*x	.	.	$R_2R_1, R_3R_1R_3R_1R_3$
36	22*2222	.	.	$R_1, R_3R_1R_3R_1R_3$
37	22*x	.	.	$R_1, R_3R_2R_3R_1R_3R_2R_3R_2$
38	***	.	.	$R_1, R_3R_1R_2R_3R_2R_1R_3$
39	**x	.	.	$R_2, R_3R_1R_3R_1R_3$
40	*xx	.	.	$R_1, R_3R_1R_2R_3R_2R_1R_3R_2$
41	*xx	.	.	$R_2, R_1R_3R_1R_2R_3R_1R_3$
42	22*x	.	.	$R_2R_1, R_3R_1R_2R_3R_2R_1R_3$
43	o22	.	.	$R_2R_1, R_3R_1R_2R_3R_2R_1R_3R_1$
44	222222	.	.	$R_2R_1, R_3R_1R_3R_1R_3R_1$
45	*xx	.	.	$R_3, R_2R_3R_1R_2R_3R_2R_3R_1$
46	3xx	16	4	$R_3R_1R_3R_1, R_1R_2R_3R_1R_2R_3R_2$
47	*3*3	.	.	$R_1, R_3R_1R_3$
48	*3*3	.	.	$R_3, R_1R_3R_1$
49	32222	.	.	$R_3R_1R_3R_1, R_2R_3R_2R_1R_3R_2$
50	6226	.	.	R_3R_1

Table 1: Subgroups of *246 commensurate with the P,D,G surfaces.

	orbifold symbol	index	conjugacy class size	subgroup generators in *246/T
51	o3	.	.	$R_3R_1R_3R_1, R_2R_3R_1R_2R_3R_2R_3R_1$
52	3xx	.	.	$R_3R_1R_3R_1, R_2R_3R_1R_2R_3R_2R_3$
53	222x	12	1	$R_3R_2R_3R_2, R_1R_3R_2R_3R_2R_1, R_1R_2R_3R_1R_3R_1R_3$
54	22222	.	.	$R_3R_2R_3R_2, R_1R_3R_2R_3R_2R_1, R_3R_1R_3R_1R_3R_1$
55	*222222	.	.	$R_2, R_3R_2R_3, R_1R_3R_2R_3R_1$
56	2xx	12	3	$R_3R_2R_3R_2, R_1R_3R_1R_3R_2R_1, R_1R_2R_3R_2R_3R_1R_3$
57	2*2222	.	.	$R_1, R_2, R_3R_1R_3R_2R_3R_2R_1R_3$
58	222x	.	.	$R_3R_2R_3R_2, R_3R_1R_3R_1R_3R_1, R_1R_2R_3R_1R_2R_3R_1$
59	2**	.	.	$R_1, R_3R_1R_3R_1R_3R_2, R_3R_1R_2R_3R_2R_1R_3R_2$
60	**22	.	.	$R_1, R_3R_2R_3$
61	o2	.	.	$R_3R_2R_3R_2, R_1R_3R_1R_3R_2R_1, R_3R_1R_3R_2R_3R_1$
62	44*	.	.	$R_1, R_3R_1R_3R_2R_1R_3$
63	2*x	.	.	$R_1, R_2R_3R_1R_2R_3R_1R_3$
64	*4444	.	.	R_2, R_3
65	222*	.	.	$R_1, R_3R_2R_3R_2$
66	22*22	.	.	$R_2, R_3R_2R_3, R_1R_3R_2R_1R_3R_1$
67	22*22	.	.	$R_2, R_3R_2R_3, R_3R_1R_3R_1R_3R_1$
68	*2*2	.	.	$R_2, R_3R_2R_3, R_3R_1R_3R_2R_3R_1$
69	*22x	.	.	$R_2, R_3R_2R_3, R_1R_3R_1R_2R_3R_1R_3$
70	**22	.	.	$R_2, R_3R_1R_3R_1R_3, R_3R_1R_2R_3R_2R_1R_3$
71	222*	.	.	$R_2, R_3R_1R_3R_1R_3R_1, R_3R_1R_2R_3R_2R_1R_3R_1$
72	2*x	.	.	$R_2, R_1R_3R_1R_2R_3R_1R_3, R_1R_3R_1R_3R_2R_1R_3$
73	2**	.	.	$R_2, R_3R_2R_3R_1$
74	44*	.	.	$R_2, R_3R_1R_3R_2R_1R_3$
75	22*22	.	.	$R_2R_1, R_3R_1R_3R_1R_3, R_3R_1R_2R_3R_2R_1R_3$
76	22222	.	.	$R_2R_1, R_3R_1R_3R_1R_3R_1, R_3R_1R_2R_3R_2R_1R_3R_1$
77	22222	.	.	$R_2R_1, R_3R_2R_3R_1$
78	2442	.	.	$R_2R_1, R_3R_1R_3R_2R_1R_3$
79	222x	.	.	$R_2R_1, R_1R_3R_1R_2R_3R_1R_3$
80	*2*2	.	.	$R_3, R_2R_3R_2, R_1R_3R_1R_3R_2R_1$
81	22*22	.	.	$R_3, R_2R_3R_2, R_1R_3R_2R_3R_2R_1$
82	*22x	.	.	$R_3, R_2R_3R_2, R_1R_2R_3R_1R_2R_3R_1$
83	*222222	.	.	$R_1, R_3R_1R_3R_1R_3, R_3R_1R_2R_3R_2R_1R_3$
84	44x	.	.	$R_3R_2, R_1R_2R_3R_1R_2R_3R_1$
85	2xx	.	.	$R_3R_2R_3R_2, R_3R_1R_3R_2R_3R_1, R_1R_2R_3R_1R_2R_3R_1$
86	4224	.	.	$R_3R_2, R_1R_3R_2R_3R_2R_1$
87	4224	.	.	$R_3R_2, R_1R_3R_1R_3R_2R_1$
88	2**	12	6	$R_1, R_3R_1R_3R_1R_3R_2, R_3R_1R_2R_3R_2R_1R_3$
89	22*22	.	.	$R_1, R_3R_1R_3R_1R_3, R_3R_1R_2R_3R_2R_1R_3R_2$
90	2*2222	.	.	$R_1, R_2, R_3R_1R_3R_1R_3$
91	*22*	.	.	$R_1, R_2, R_3R_1R_2R_3R_2R_1R_3$
92	2323	8	1	$R_3R_1R_3R_1, R_3R_2R_3R_2$
93	6222	8	4	$R_3R_1, R_2R_3R_2R_1R_3R_2$
94	62x	.	.	$R_3R_1, R_1R_2R_3R_1R_2R_3R_2$
95	*3x	.	.	$R_3, R_1R_3R_1, R_1R_2R_3R_1R_2R_3R_2$
96	*6262	.	.	R_1, R_3
97	22*3	.	.	$R_1, R_3R_1R_3, R_2R_3R_2R_1R_3R_2$
98	*3x	.	.	$R_1, R_3R_1R_3, R_2R_3R_1R_2R_3R_2R_3$
99	22*3	.	.	$R_3, R_1R_3R_1, R_2R_3R_2R_1R_3R_2$
100	2*222	6	1	$R_2, R_3R_2R_3, R_1R_3R_2R_3R_1, R_3R_1R_3R_1R_3R_1$

12

Table 1: Subgroups of *246 commensurate with the P,D,G surfaces.

	orbifold symbol	index	conjugacy class size	subgroup generators in *246/T
101	*22222	6	3	$R_1, R_2, R_3R_1R_3R_1R_3, R_3R_1R_2R_3R_2R_1R_3$
102	*22222	.	.	$R_1, R_2, R_3R_2R_3$
103	*2442	.	.	$R_1, R_3R_2R_3, R_3R_1R_3R_1R_3$
104	2*222	.	.	$R_1, R_3R_2R_3R_2, R_3R_1R_3R_1R_3$
105	**2	.	.	$R_1, R_3R_2R_3, R_3R_1R_3R_1R_3R_2$
106	4*22	.	.	$R_1, R_2, R_3R_1R_3R_2R_1R_3$
107	*4422	.	.	$R_2, R_3, R_1R_3R_2R_3R_1$
108	2*44	.	.	$R_2, R_3, R_1R_3R_2R_1R_3R_1$
109	24*	.	.	$R_2, R_3R_2R_3R_1, R_3R_1R_3R_1R_3R_1$
110	24*	.	.	$R_1, R_3R_2R_3R_2, R_3R_1R_3R_1R_3R_2$
111	22*2	.	.	$R_2, R_3R_2R_3, R_1R_3R_2R_1R_3R_1, R_3R_1R_3R_1R_3R_1$
112	**2	.	.	$R_2, R_3R_2R_3R_1, R_3R_1R_3R_1R_3$
113	22*2	.	.	$R_2R_1, R_3R_2R_3R_1, R_3R_1R_3R_1R_3$
114	2224	.	.	$R_2R_1, R_3R_2R_3R_1, R_3R_1R_3R_1R_3R_1$
115	3*22	4	1	$R_2, R_3R_1R_3R_1$
116	434	.	.	$R_3R_2, R_1R_3R_2R_1$
117	2*33	.	.	$R_1, R_3R_1R_3, R_3R_2R_3R_2$
118	2322	.	.	$R_2R_1, R_3R_1R_3R_1$
119	*3232	.	.	$R_3, R_1R_3R_1, R_2R_3R_2$
120	266	.	.	$R_3R_1, R_2R_3R_2R_1$
121	23x	.	.	$R_1R_2R_3, R_1R_3R_2$
122	2*62	4	4	$R_1, R_3, R_2R_3R_2R_1R_3R_2$
123	*2422	3	3	$R_1, R_2, R_3R_2R_3, R_3R_1R_3R_1R_3$
124	*2232	2	1	$R_1, R_2, R_3R_1R_3$
125	*434	.	.	$R_2, R_3, R_1R_3R_1$
126	6*2	.	.	R_2, R_3R_1
127	*662	.	.	$R_1, R_3, R_2R_3R_2$
128	4*3	.	.	R_1, R_3R_2
129	2*32	.	.	$R_2R_1, R_3, R_1R_3R_1$
130	462	.	.	R_2R_1, R_3R_1
131	*642	1	1	R_1, R_2, R_3